

# Numerical analysis of bushing of car stabilizer

Jakub Javorik, and Ondrej Bilek

**Abstract**—The goal of this work is to create numerical model, which will be used for design and optimization of a rubber bushing of stabilizer bar. Thanks this model we are able to predict the mechanical behavior of the bushing. To get material constants for the model, the material of bushing (rubber) was tested in special deformations modes. A hyperelastic material model was set and it was implemented into the numerical model of the bushing. Critical points in the construction of bushing were revealed by the analysis of the numerical model.

**Keywords**— bushing, hyperelasticity, numerical model, stabilizer bar.

## I. INTRODUCTION

THE stabilizer bar (Fig. 1) is an important part of a car suspension. It is intended to force each side of the vehicle to lower, or rise, to similar heights, to reduce the sideways tilting of the vehicle on curves, sharp corners, or large bumps. One of the factors which influence the function and behavior of the stabilizer bar is a way in which it is connected with the car frame. This connection must be able to absorb quite large deformation of the stabilizer bar. Therefore the rubber bushings are commonly used to clamp stabilizer bar and to fasten it to the car frame (Fig. 2). To design stabilizer bar bushing properly we need to predict the bushing behavior accurately. The numerical model [1]-[19] of the bushing was created and the analysis of its behavior is described in this paper. Main goal of the work was to analyze the radial stiffness of the bushing.

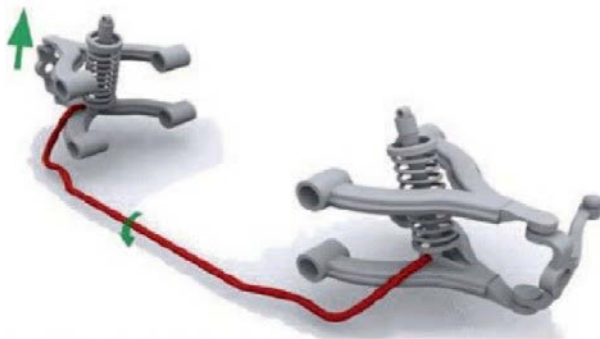


Fig. 1 car stabilizer bar [20]

J. Javorik is with the Tomas Bata University in Zlin, nam. T. G. Masaryka 5555, 760 01 Zlin, Czech Republic (phone: +420 576 035 151; fax: +420 576 035 176; e-mail: javorik@ft.utb.cz).

O. Bilek is with the Tomas Bata University in Zlin, nam. T. G. Masaryka 5555, 760 01 Zlin, Czech Republic (e-mail: bilek@ft.utb.cz).

## II. MATERIAL AND METHODS

### A. Geometry of Bushing

The scheme of half cut stabilizer bar bushing is shown in the Fig. 3. The bushing consists of three main parts: two rubber parts (a) and (b), and steel bracket (c). Rubber parts are mounted on the stabilizer bar (d) and then together with the stabilizer bar they are fixed by the steel bracket (c) to the car frame. Both rubber parts of the bushing are reinforced by the aluminum core (e). There are eight holes in each core plate for better fixation in the elastomer (Fig. 4).

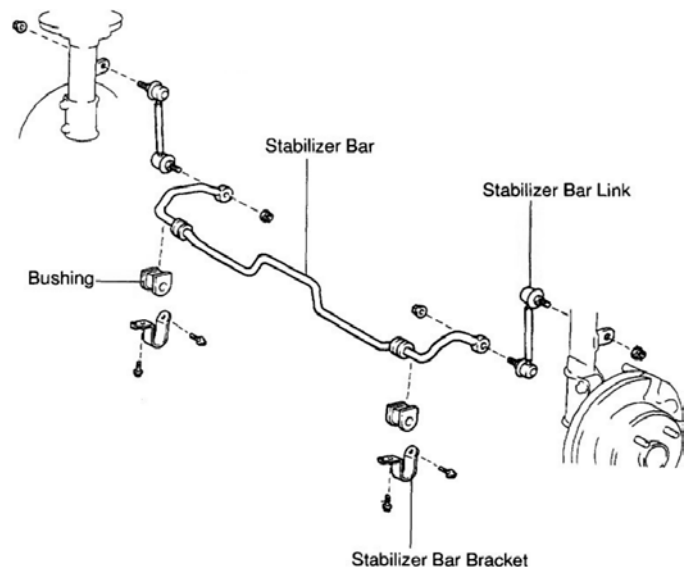


Fig. 2 stabilizer bar attachment [21]

### B. Material

We need to characterize two materials of bushing:

- material of elastomer: NR 60±3 Sh A
- material of bushing core: EN AW-ALMg3-H46.

Material of the core (EN AW-ALMg3-H46) is standardized type of aluminum alloy and we can get data from common material databases. Young modulus of this material is  $E=70000$  MPa and Poisson ratio  $\mu=0.3$ . Contrary to the core, to characterize the rubber, from which the elastomer part of the bushing is made, we need to test the mechanical properties of this material. This material was tested in three basic deformation modes that are used to characterize a hyperelastic material [22]-[29]. These tests are: uniaxial tension, equibiaxial tension and pure shear (Fig. 5).

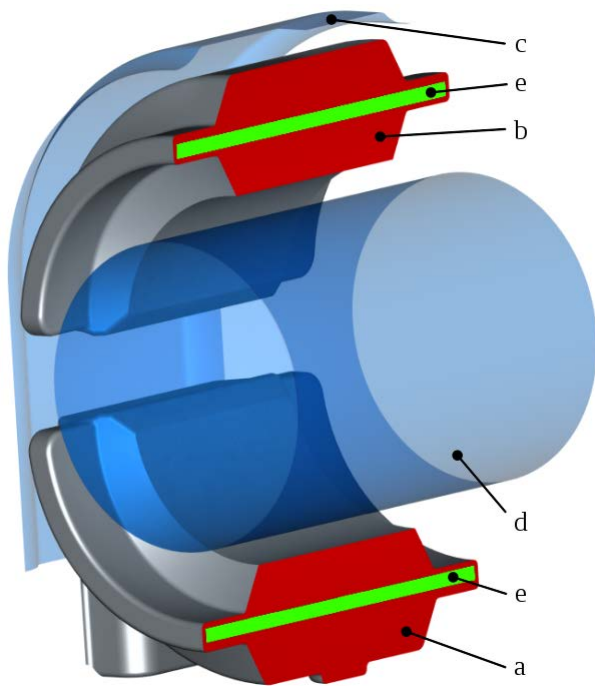


Fig. 3 half cut scheme of the stabilizer bar bushing



Fig. 4 shape of the bushing core

*Uniaxial tension test of elastomer*

Uniaxial tension tests of elastomer [30], according ISO 37 standard, was performed to determine the hyperelastic material parameters. The test was performed on an universal tensile testing machine. A 1.5 mm thick dumb-bell shaped specimen (type 1A – ISO 37) was used (Fig. 6). Stress/strain curve was measured during the whole range of loading. Specimens were loaded up to deformation of  $\epsilon=1.5$ .

*Equibiaxial tension test of elastomer*

A bubble inflation technique was used to characterize the elastomer in the equibiaxial tension [31]-[36].

The bubble inflation technique involves a uniform circular specimen clamped at the rim and inflated by increasing the air pressure on one side. The specimen deforms into the shape of a bubble (Fig. 7 and 8). The inflation of the specimen results

in an equibiaxial stretching near the pole of the bubble and a planar tension near the rim.

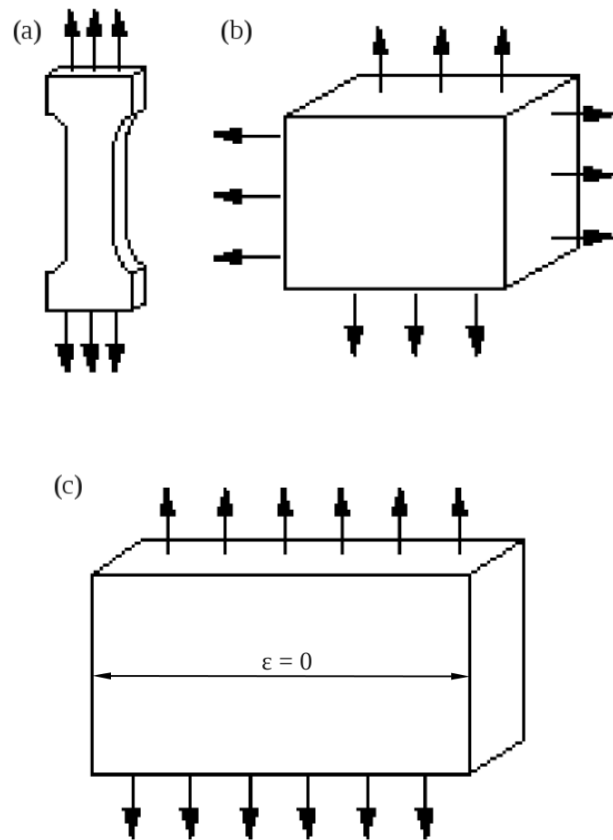


Fig. 5 three basic deformation modes of elastomer tests



Fig. 6 1A type of uniaxial tension test specimen (ISO 37)

Due to the spherical symmetry at the bubble pole, where  $\sigma$  represents the hoop stress  $\sigma_{\theta\theta}=\sigma_{\phi\phi}$ . Then the Cauchy stress tensor can be expressed as

$$\sigma = \begin{bmatrix} \sigma_{rr} & 0 & 0 \\ 0 & \sigma_{\theta\theta} & 0 \\ 0 & 0 & \sigma_{\theta\theta} \end{bmatrix}. \tag{1}$$

As the thickness  $t$  of the inflated specimen is small compared with its radius of curvature  $r$ , the thin shell assumption is appropriate, allowing us to neglect the radial stress  $\sigma_{rr}$  in comparison with the stress  $\sigma_{\theta\theta}$ . In addition we equate  $\sigma_{\theta\theta}$  to the thickness-averaged hoop stress, which leads to

$$\sigma_{\theta\theta} = \frac{pr}{2t}, \tag{2}$$

where  $p$  is the differential inflation pressure inside the bubble,  $r$  is radius of curvature of the specimen and  $t$  is the specimen thickness (Fig. 7).

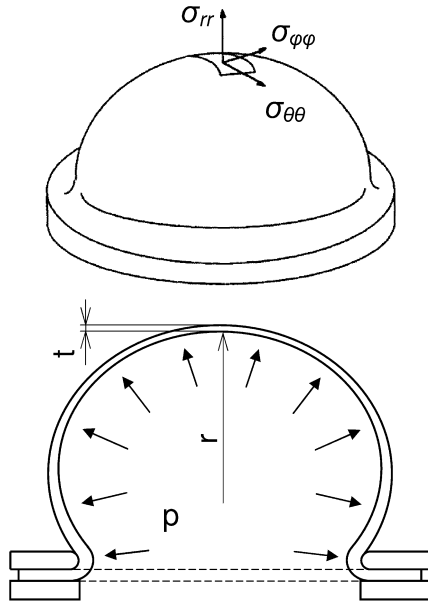


Fig. 7 the bubble inflation technique



Fig. 8 inflated equibiaxial specimen with white stripes

Considering the material incompressibility, the thickness of the inflated specimen can be expressed as

$$t = \frac{t_0}{\lambda_{\theta\theta}^2}, \tag{3}$$

where  $t_0$  is the initial specimen thickness (unloaded state). The stretch  $\lambda_{\theta\theta}$  at the pole of the inflated specimen must be measured. Generally, the stretch  $\lambda$  is the ratio between the actual length  $l$  and the initial length  $l_0$ , or

$$\lambda = \frac{l}{l_0}. \tag{4}$$

Using a video camera, the stretch  $\lambda_{\theta\theta}$  and the radius of curvature  $r$  were measured.

Substituting equation (3) into the equation (2) the hoop stress becomes

$$\sigma_{\theta\theta} = \frac{pr\lambda_{\theta\theta}^2}{2t_0}. \tag{5}$$

To compute the hoop stress  $\sigma_{\theta\theta}$  from the (5) the pressure  $p$  inside the bubble, the radius of curvature of the bubble  $r$ , and the stretch  $\lambda_{\theta\theta}$  at the bubble pole must be measured during the inflation. To characterize the hyperelastic material behavior, knowledge of the entire stress/strain curve is necessary (Fig. 9). Thus, the above mentioned parameters were recorded continuously during the whole test.

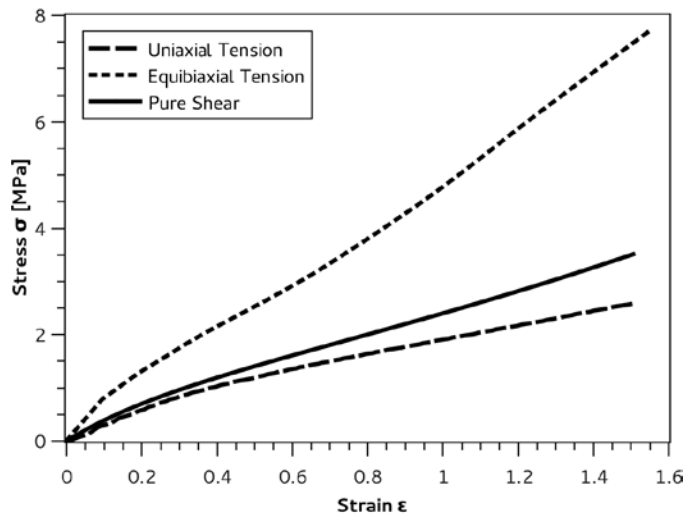


Fig. 9 results of tests of bushing elastomer

Specimens with thickness  $t_0=1.5$  mm were tested, and diameter of the hole through which the bubble is inflated was 50 mm. Pressure was measured using a digital manometer. The inflation of the specimen was recorded using a video camera and the stretch and bubble radius were obtained by analyzing the resulting video. Finally, the manometer display appeared in the video images, so relating the pressure to every stretch or radius value was simple and reliable.

To determine the bubble radius and stretch from the video images, two stripes were drawn on the specimen surface, identifying two points on the bubble silhouette. Tracing an arc through these points and the pole of the bubble allows the determination of the radius and the length of the arc (Fig. 8).

*Pure shear test of elastomer*

In this test, the specimen is loaded by tension similarly like in the uniaxial tension test. Important difference is in the

boundary conditions during the test. Cross-section area of the uniaxial specimen (Fig. 3a) is not constrained and it can freely contract in its both dimensions during the loading. Contrary uniaxial tension, pure shear specimen can change only its thickness during the test. Its width will remain constant during the whole range of loading (Fig. 3c). To fulfill this condition it is necessary that the height of the sample is substantially smaller than its width and that both longitudinal edges of specimen are firmly clamped in the long clamps which prevent change of the specimen width (Fig. 10).



Fig. 10 pure shear test specimen in long clamps [37]

### C. Hyperelasticity

A hyperelastic material constants were set up from results of tests presented above. Currently a number of hyperelastic material models are available they vary in defining the strain energy density function  $W$  [38]-[43].  $W$  is a function of a deformation tensor, whose derivative with respect to a strain component determines the corresponding stress component. Explicitly,

$$S_{ij} = \frac{\partial W}{\partial C_{ij}}, \quad (6)$$

where  $S_{ij}$  are components of the 2<sup>nd</sup> Piola Kirchhoff stress tensor and  $C_{ij}$  are components of the right Cauchy-Green deformation tensor [44], that will be as follows

$$C_{ij} = \begin{bmatrix} \lambda_1^2 & 0 & 0 \\ 0 & \lambda_2^2 & 0 \\ 0 & 0 & \lambda_3^2 \end{bmatrix}. \quad (7)$$

Hyperelastic models are usually named after their authors.

Some of the best known and most used models are: Neo-Hookean, Mooney-Rivlin, Yeoh, Second Order Invariant, James-Green-Simpson, Ogden, Gent, Arruda-Boyce [45]-[51].

### D. Numerical Model of the Bushing

An advanced nonlinear "Finite Element Method" (FEM) system was used for numerical model creation and for the analysis. With regard to the symmetric shape of the bushing and to the symmetry of loads and boundary conditions (which will be described below) we can reduce the geometry of the numerical model to one quarter of original shape (Fig. 11). First plane of symmetry is normal to the axis of stabilizer bar and it is placed in the center of the bushing. Second symmetry plane coincides with the stabilizer bar axis and is perpendicular to the first plane (Fig. 11). Quarter model has four parts: bottom bushing part, top bushing part, stabilizer bar and bracket. Aluminum cores are positioned inside the top and bottom bushing parts (they are not shown in the Fig. 11).



Fig. 11 geometry of the numerical (quarter) model

In the model, the rubber parts and aluminum core were created of the "Four Node Tetrahedron Finite Elements" [52]. The stabilizer bar and bracket are created as rigid bodies. Elastomer and core share nodes on their boundaries and therefore they are fixed together.

Material constants of aluminum are given above. For elastomer an appropriate hyperelastic material model had to be set. Using results from uniaxial tension, equibiaxial tension and pure shear tests of elastomer, material constants of above mentioned hyperelastic models were computed. The closest agreement with experimental data (i.e. minimal error) showed a "2<sup>nd</sup> Order Invariant" hyperelastic model [53]. The strain

energy density function  $W$  of this model is as follows:

$$W = c_{10}(I_1 - 3) + c_{01}(I_2 - 3) + c_{11}(I_1 - 3)(I_2 - 3) + c_{20}(I_1 - 3)^2 \quad (8)$$

where  $I_1$  and  $I_2$  are first and second invariants of right Cauchy-Green deformation tensor defined as (7). There is the comparison of this model and experiment in the Fig. 12. Computed material constants of this model are:  $c_{10}=0.23264$  MPa,  $c_{01}=0.16711$  MPa,  $c_{11}=-0.0060978$  MPa and  $c_{20}=0.01475$  MPa.

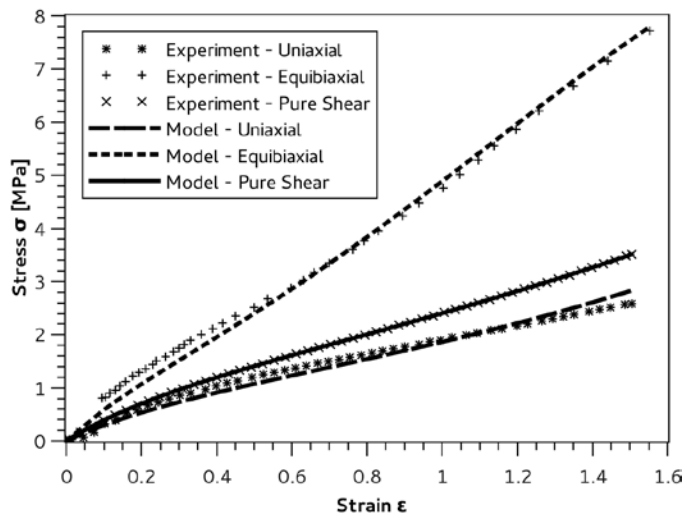


Fig. 12 comparison of experimental data and the 2<sup>nd</sup> Order Invariant hyperelastic model

### E. Loads and boundary conditions

To be as close as possible to reality, the loads are applied in two steps. The first step can be considered as a "Mounting of bushing on the stabilizer bar". During this step some deformation and stress of the bushing occurs and the model is in the state of initial "preload" at the end of the first step. During the second step required load is applied to the stabilizer bar.

#### First load step

There is partially cut scheme of a real actuator bushing shown in Fig. 13. Contrary the presented numerical model there is a polyamide support. The bottom part of elastomer is fixed in this support and the support together with the bracket is fixed to the car frame. It means that the support can be replaced by the null displacement boundary condition on the surfaces of bottom elastomer in the numerical model. Therefore all three degrees of freedom of displacement were constrained on surfaces of bottom part of elastomer. These surfaces are shown in Fig. 14.

A symmetry conditions are set on the symmetry planes (shown in Fig. 11) as a null displacement in planes normal directions. There is a contact defined between two rubber parts of bushing, between these parts and the stabilizer bar, and between these parts and bracket. No friction is defined

between contact bodies.

The bushing mounting is done by the displacement of the bracket. The bracket moves down against to bottom part of bushing (i.e. radial direction). During this motion the bracket touch the top part of bushing first, and then shift it to the stabilizer bar. Stabilizer bar can move only vertically (other two displacements are not allowed), and thus it is pushed into the bottom part of bushing and is clamped from the top by other part of bushing and by bracket.

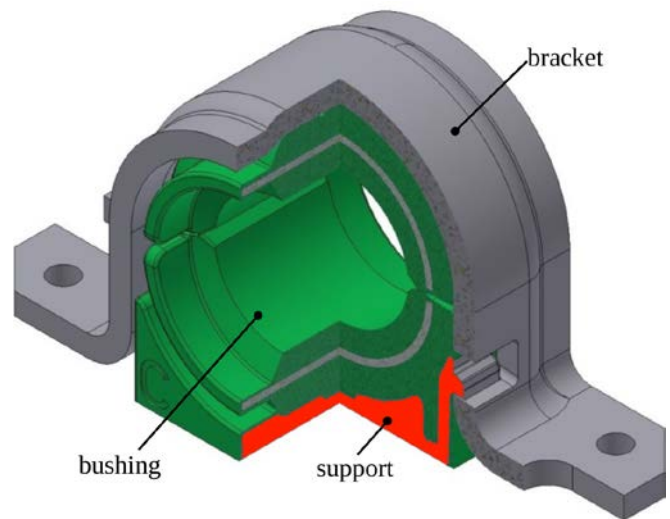


Fig. 13 scheme of the bushing with the support

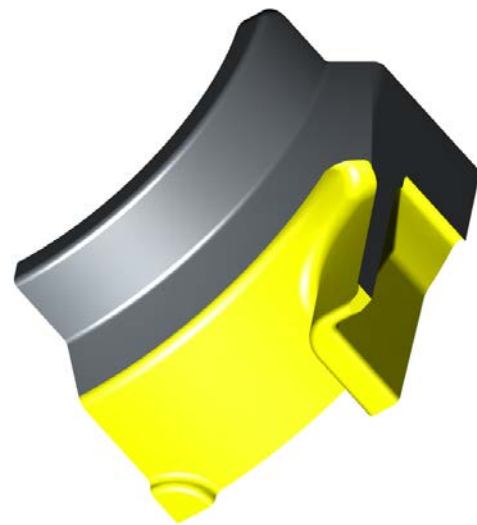


Fig. 14 surfaces of bushing bottom part with null displacement

#### Second load step

At the beginning of this step, "glue" contact type is defined between rubber parts and the rigid stabilizer bar. It means that stabilizer bar is fixed on the surfaces of the bushing during whole second step. It should be in accordance with reality when bushing is fastened on stabilizer bar. Vertical radial force  $F=2000$  N is gradually applied on the stabilizer bar

during second step (Fig. 15). It should be remembered that this force is applied only to quarter model and thus the load of full model is four times larger (8000 N). Rigid bracket will remain in its final position from the first step and will not move during the second step.

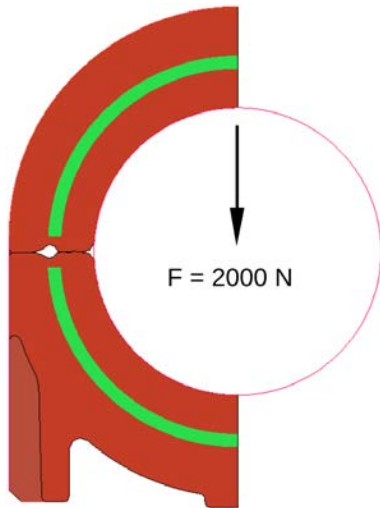


Fig. 15 stabilizer bar loading during the second load step

III. RESULTS AND DISCUSSION

The main result is "Radial Stiffness" of the bushing. To compute this parameter the "loading radial force / radial displacement of stabilizer bar" relation was monitored (Fig. 16). The stiffness was determined in the range of loading from  $F=4000$  N to  $F=8000$  N (as well as in the practical tests of a real bushing). Values of force above are given for the whole bushing (i.e. 1000 N and 2000 N for the quarter numerical model). The final value of the Radial Stiffness of the model is 11168 N/mm. Average value from the tests of a real bushing is 11190 N/mm.

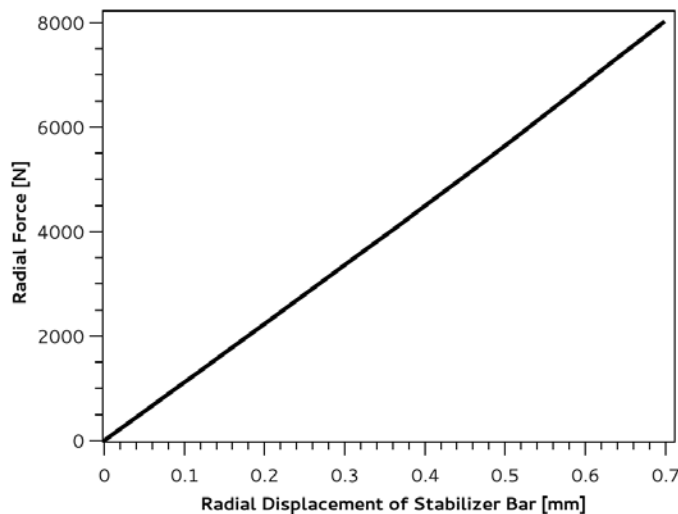


Fig. 16 force/displacement curve of numerical model analysis

There is a Von Mises equivalent of strain in the model shown in the Fig. 17. The deformation of the bushing at the end of the first load step (time=1.0) is shown in the first picture (Fig. 17a) and the deformation under the final radial loading of  $F=8000$  N at the end of the second load step (time=2.0) is shown in the second picture (Fig. 17b). We can see critical point with the maximum strain of  $\epsilon=1.06$  at the end of second step (maximum at the end of first step was  $\epsilon=0.71$ ). This point is shown in the detail in the Fig. 18.

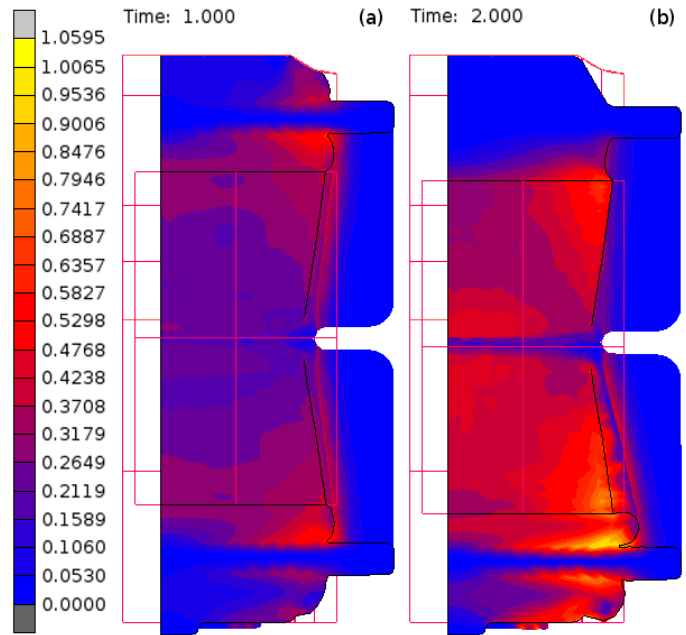


Fig. 17 Von Mises equivalent of strain in the model

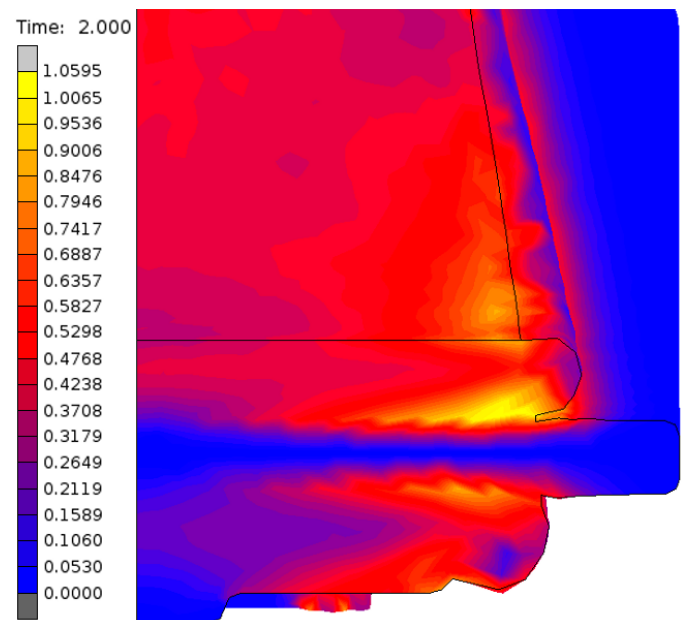


Fig. 18 maximum of Von Mises equivalent of strain in the model

Contrary the strain, the stress distribution is absolutely different. Stress is concentrated on the aluminum core and in

its vicinity (Fig. 19 and 20). There is shown bushing including core in Fig. 19, and the only rubber part of the bushing in the Fig. 20. Because the stresses in the aluminum core do not reach the strength (stress limit) of the material, the core is not studied more.

observed from outside. Thus we need special diagnostic methods to find such failings.

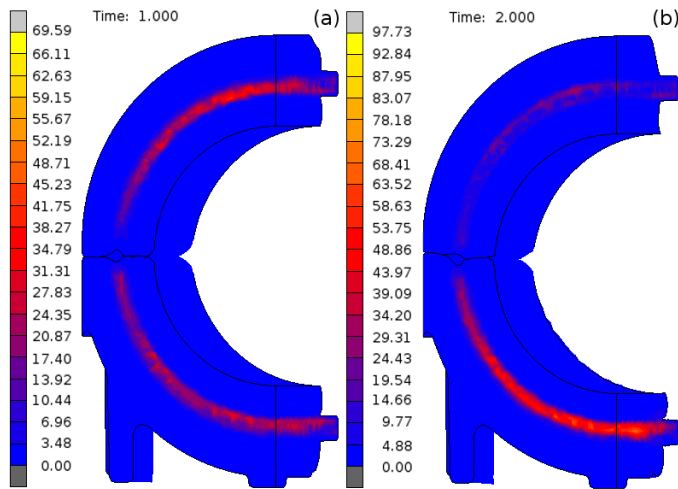


Fig. 19 Von Mises equivalent of stress [MPa]

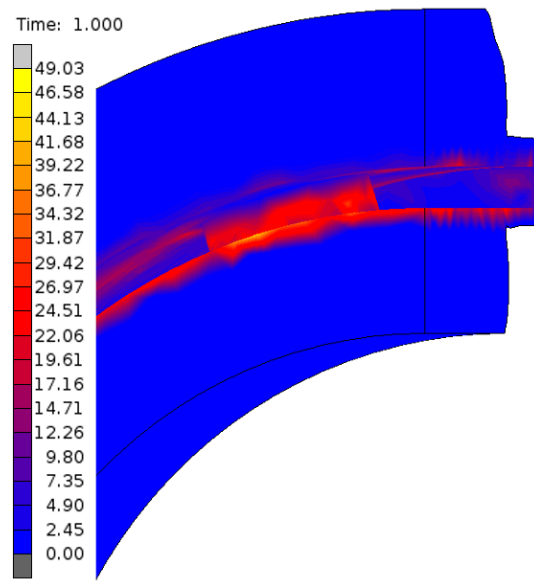


Fig. 21 maximum of Von Mises equivalent of stress [MPa] in elastomer at the end of first load step

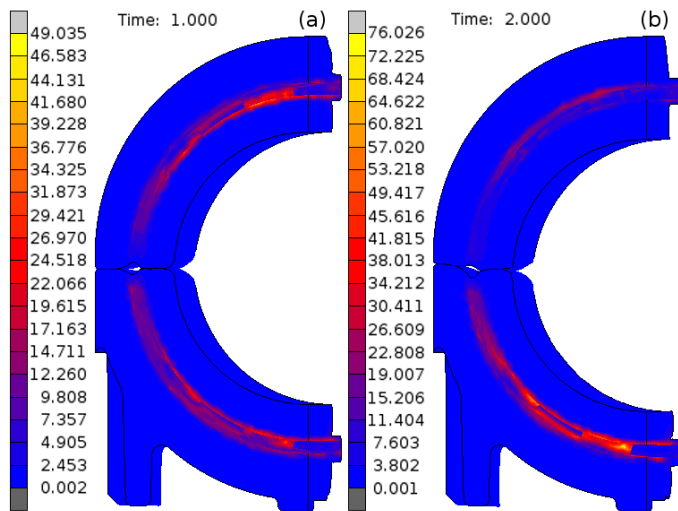


Fig. 20 Von Mises equivalent of stress [MPa] - only in elastomer

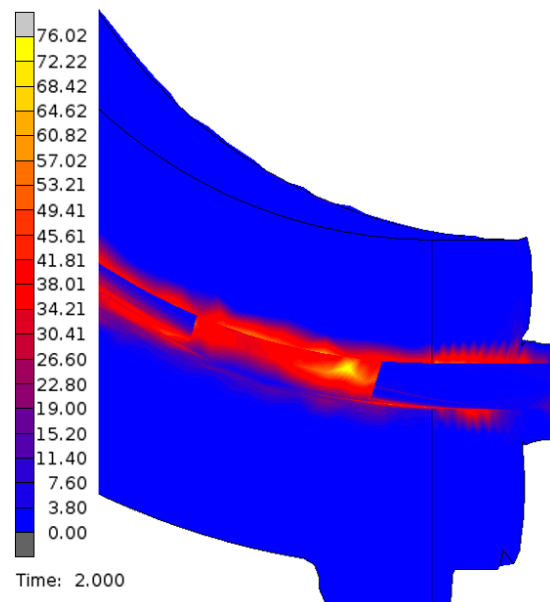


Fig. 22 maximum of Von Mises equivalent of stress [MPa] in elastomer at the end of second load step

We can see that the extreme stresses in the rubber part are located in the spaces of the core holes and that the stress values are very high here even at the end of first load step in time=1.0 (Fig. 21) and they reach their maximum at the end of the second load step (Fig. 22). The reason of this is that the elastomer has no space where to run out during the loading (it is closed in the core hole). Similar situation occurs on the core surfaces where the deformation of the elastomer is constrained by the aluminum core. It means that the critical point of the bushing is the surface of the core (especially in the holes) where the stress is concentrated during the loading, and therefore there is a high risk of tearing off the rubber from the core. Next risk, resulting from this issue, is the fact that this defect of bushing is closed inside the device and can not be

IV. CONCLUSION

Based on the tests of material the appropriate hyperelastic model of elastomer was determined and the material constants were computed. Using this model, we are able to predict the behavior of the bushing under the radial loading. Even next modes of loading can be analyzed by this model and these analyses were carried out but they are outside the scope of this article and they will be published later. The suitability of the

numerical model was approved by close agreement with the experiment of real bushing. Analysis of the model revealed the critical points of the bushing and its results will be used to future shape optimization of the product. This optimization should minimize the risk of the tearing of rubber from aluminum core which will lead to extension of the bushing working life.

## REFERENCES

- [1] A. Arghiropol, and C. Rotaru, "Overview of the 2D and 3D finite element studies versus experimental results of a solid propellant engine performances under cycling loading effect," *Int. J. of Math. Comput. in Simul.*, vol. 4, pp. 42-49, 2010.
- [2] S. Amornsamankul, K. Kaorapong, and B. Wiwatanapataphee, "Three-dimensional simulation of femur bone and implant in femoral canal using finite element method," *Int. J. of Math. Comput. in Simul.*, issue 4, vol. 4, pp. 171-178, 2010.
- [3] M. C. Popescu, and M. E. Mastorakis, "Optimal flow control of a three tank system," *Int. J. of Math. Comput. in Simul.*, vol. 3, pp. 179-186, 2009.
- [4] A. Ionescu, M. Calbureanu, and M. Negru, "Static and dynamic simulation in the seismic behavior of a building structure using ANSYS program," *Int. J. Mech.*, vol. 7, pp. 210-217, 2013.
- [5] J. Javorik, and M. Stanek, "The shape optimization of the pneumatic valve diaphragm," *Int. J. Math. Comput. Simul.*, vol. 5, pp. 361-369, 2011.
- [6] J. Javorik, and M. Stanek, "The numerical simulation of the rubber diaphragm behavior," in *Recent Res. in Autom. Control : 13<sup>th</sup> WSEAS Int. Conf. on Autom. Control, Modell. & Simul.*, Lanzarote, Spain: WSEAS Press, 2011, pp. 117-120.
- [7] L. J. Billings, and R. Shepherd, "The modeling of layered steel/elastomer seismic base isolation bearings," in *Proc. 1992 MARC User Conf.*, Monterey, CA, USA, 1992.
- [8] O. Suba, and L. Sykorova, "Transient of thermal stresses in printed circuit boards," *Int. J. Mech.*, vol. 5, pp. 226-233, 2011.
- [9] L. Sykorova, and O. Suba, "The transient temperature field simulation of polymeric materials during laser machining," *Int. J. Mech.*, vol. 5, pp. 234-241, 2011.
- [10] M. Stanek, D. Manas, M. Manas, and O. Suba, "Optimization of injection molding process," *Int. J. Math. Comput. Simul.*, vol. 5, pp. 413-421, 2011.
- [11] M. Stanek, D. Manas, M. Manas, and J. Javorik, "Simulation of injection molding process by Cadmould Rubber," *Int. J. Math. Comput. Simul.*, vol. 5, pp. 422-429, 2011.
- [12] O. Suba, L. Sykorova, S. Sanda, and M. Stanek, "Modeling of thermal stress in printed circuit boards," in *Recent Res. in Autom. Control : 13<sup>th</sup> WSEAS Int. Conf. on Autom. Control, Modell. & Simul.*, Lanzarote, Spain: WSEAS Press, 2011, pp. 173-176.
- [13] O. Suba, L. Sykorova, S. Sanda, and M. Stanek, "Stress-state modelling of injection-molded cylindrical bosses reinforced with short fibers," in *Recent Res. in Autom. Control: 13<sup>th</sup> WSEAS Int. Conf. on Autom. Control, Modell. & Simul.*, Lanzarote, Spain: WSEAS Press, 2011, pp. 177-179.
- [14] L. Sykorova, O. Suba, M. Malachova, and J. Cerny, "Temperature field simulation of polymeric materials during laser machining using COSMOS/M software," in *Recent Res. in Autom. Control : 13<sup>th</sup> WSEAS Int. Conf. on Autom. Control, Modell. & Simul.*, Lanzarote, Spain: WSEAS Press, 2011, pp. 180-184.
- [15] M. Stanek, D. Manas, M. Manas, and J. Javorik, "Simulation of injection molding process," in *Recent Res. in Autom. Control : 13<sup>th</sup> WSEAS Int. Conf. on Autom. Control, Modell. & Simul.*, Lanzarote, Spain: WSEAS Press, 2011, pp. 231-234.
- [16] M. Stanek, D. Manas, M. Manas, and O. Suba, "Optimization of injection molding process by MPX," in *Recent Res. in Autom. Control : 13<sup>th</sup> WSEAS Int. Conf. on Autom. Control, Modell. & Simul.*, Lanzarote, Spain: WSEAS Press, 2011, pp. 212-216.
- [17] M. S. Salleh, M. Z. Omar, J. Syarif, M. N. Mohammed, and K. S. Alhawari, "Thermodynamic simulation on thixofomability of aluminium alloys for semi-solid metal processing," *Int. J. of Math. Comput. in Simul.*, vol. 7, pp. 286-293, 2013.
- [18] D. Samek, and J. Javorik, "Numerical analysis of shape stability of rubber boot," *Int. J. Mech.*, vol. 7, pp. 293-301, 2013.
- [19] K. Frydrysek, R. Janco, and H. Gondek, "Solutions of beams, frames and 3D structures on elastic foundation using FEM," *Int. J. Mech.*, vol. 7, pp. 362-369, 2013.
- [20] C. Longhurst. (2014, June, 16). *The Suspension Bible* [Online]. Available: [http://www.carbibles.com/suspension\\_bible\\_pg4.html](http://www.carbibles.com/suspension_bible_pg4.html)
- [21] D. Sestak, "Numerical model of rubber bushing of car stabilizer," (in czech) M.S. thesis, Dept. Prod. Eng., Thomas Bata Univ., Zlin, Czech Republic, 2014.
- [22] R. W. Ogden, *Non-linear Elastic Deformations*. New York: Dover Publications, 1997.
- [23] A. N. Gent, *Engineering with Rubber*. Munich: Hanser, 2001.
- [24] N. Huber, and C. Tsakmakis, "Finite deformation viscoelasticity laws," *Mech. Mater.*, vol. 32, pp. 1-18, 2000.
- [25] A. N. Gent, "Extensibility of rubber under different types of deformation," *J. Rheol.*, vol. 49, pp. 271-275, 2005.
- [26] L. R. G. Treloar, "Mechanics of rubber elasticity," *J. Polym. Sci. Pol. Symp.*, vol. 48, pp. 107-123, 1974.
- [27] L. R. G. Treloar, *The Physics of Rubber Elasticity*. Oxford: Clarendon Press, 1975.
- [28] R. H. Finney, and A. Kumar, "Development of material constants for nonlinear finite element analysis," *Rubber Chem. Technol.*, vol. 61, pp. 879-891, 1988.
- [29] O. H. Yeoh, "Characterization of elastic properties of carbon black filled rubber vulcanizates," *Rubber Chem. Technol.*, vol. 63, pp. 792-805, 1990.
- [30] L. P. Smith, *The Language of Rubber*. Oxford: Butterworth-Heinemann, 1993.
- [31] J. Javorik, and Z. Dvorak, "Equibiaxial test of elastomers," *KGK-Kautsch. Gummi Kunstst.*, vol. 60, pp. 608-610, 2007.
- [32] W. D. Kim, W. S. Kim, C. S. Woo, and H. J. Lee, "Some considerations on mechanical testing methods of rubbery materials using nonlinear finite element analysis," *Polym. Int.*, vol. 53, pp. 850-856, 2004.
- [33] L. Chevalier, and Y. Marco, "Tools for multiaxial validation of behavior laws chosen for modeling hyperelasticity of rubber-like materials," *Polym. Eng. Sci.*, vol. 42, pp. 280-298, 2002.
- [34] N. Reuge, F. M. Schmidt, Y. Le Maout, M. Rachik, and F. Abbe, "Elastomer biaxial characterization using bubble inflation technique. I: Experimental investigations," *Polym. Eng. Sci.*, vol. 41, pp. 522-531, 2001.
- [35] J. Javorik, and Z. Dvorak, "The testing of hyperelastic properties of the rubber materials," *Chem. Listy*, vol. 105, pp. 273-274, 2011.
- [36] J. E. Mark, "Some unusual elastomers and experiments on rubberlike elasticity," *Prog. Polym. Sci.*, vol. 28, pp. 1205-1221, 2003.
- [37] *Experimental Elastomer Analysis*, MSC Software Corporation, Santa Ana, CA, 2010, pp. 68-69.
- [38] R. S. Rivlin, and K. N. Sawyers, "Strain-energy function for elastomers," *Tran. Soc. Rheol.*, vol. 20, pp. 545-557, 1976.
- [39] M. H. B. M. Shariff, "Strain energy function for filled and unfilled rubberlike material," *Rubber Chem. Technol.*, vol. 73, pp. 1-21, 2000.
- [40] G. A. Holzapfel, *Nonlinear Solid Mechanics*. Chichester: Wiley, 2000.
- [41] M. Bercovier, E. Jankovich, F. Leblanc, and M. A. Durand, "A finite element method for the analysis of rubber parts: Experimental and analytical assessment," *Comput. Struct.*, vol. 14, pp. 384-391, 1981.
- [42] J. E. Mark, B. Erman, and F. R. Eirich, *Science and Technology of Rubber*. New York: Academic Press, 1994.
- [43] A. Boukamel, L. Laiarinandrasana, S. Méo, and E. Verron, *Constitutive Models for Rubber V*. London: Taylor & Francis, 2008.
- [44] P. C. Chou, and N. J. Pagano, *Elasticity: Tensor, Dyadic, and Engineering Approaches*. New York: Dover, 1992.
- [45] P. Haupt, and A. Lion, "On finite linear viscoelasticity of incompressible isotropic materials," *Acta Mech.*, vol. 159, pp. 87-124, 2002.
- [46] A. N. Gent, "A new constitutive relation for rubber," *Rubber Chem. Technol.*, vol. 69, pp. 781-785, 2001.
- [47] R. S. Rivlin, "Finite elasticity theory as a model in the mechanics of viscoelastic materials," *J. Polym. Sci. Pol. Symp.*, vol. 48, pp. 125-144, 1974.
- [48] O. H. Yeoh, "Some forms of the strain energy function for rubber," *Rubber Chem. Technol.*, vol. 66, pp. 754-771, 1993.
- [49] R. A. Brockman, "On the use of the Blatz-Ko constitutive model for nonlinear finite element analysis," *Comput. Struct.*, vol. 24, pp. 607-611, 1986.

- [50] E. M. Arruda, and M. C. Boyce, "A three-dimensional constitutive model for the large stretch behavior of rubber elastic materials," *J. Mech. Phys. Solids*, vol. 41, pp. 389-412, 1993.
- [51] M. C. Boyce, "Direct comparison of the Gent and the Arruda-Boyce constitutive models of the rubber elasticity," *Rubber Chem. Technol.*, vol. 69, pp. 781-785, 1996.
- [52] A. F. Bower, *Applied Mechanics of Solids*. New York: CRC Press, 2009.
- [53] S. Cescotto, and G. Fonder, "A finite element approach for large strains of nearly incompressible rubber-like materials," *Int. J. Solids Struct.*, vol. 15, pp. 589-605, 1979.